Limits of 4-Wire 3-Level NPC topology for Hybrid Energy Storage System and power quality improvement in microgrids

[1, 2] Quentin TABART, [1] Ionel VECHIU, [1] Aitor ETXEBERRIA, [2] Seddik BACHA
[1]ESTIA, F-64210, Bidart, France, [2]G2ELab, F-38000, Grenoble, France,

Abstract– In this paper, the limits of a 4-Wire 3-Level Neutral Point Clamped (4W-3L-NPC) inverter used as the only interface to integrate a renewable energy source and a Hybrid Energy Storage System (HESS) into a microgrid are under investigation. The power flow management of the DC side is based on a Second Order Sliding Mode Controller that aims to realize a frequency decoupling of load and renewable energy disturbance. The investigation focuses on the power flow division capabilities among a vanadium redox flow battery and a lithium ion battery composing the HESS. Both simulations and experiments will support the limits analysis as well as the proposed control strategy.

Keywords— Hybrid Energy Storage System, Multilevel Inverter, Microgrids, Renewable Energy Source, Distributed Generation.

1. INTRODUCTION

The constant increase of Renewable Energy Sources (RES) integration due to the limitation of fossil fuel and the social awareness on global warming may lead to stability and power quality issues in weak grids such as microgrids. To limit these drawbacks, renewable power plants are nowadays asked to provide ancillary services to the utility grid, such as frequency and voltage regulation. However due to the stochastic nature of RES, like wind and solar energy, the use of Energy Storage Systems (ESSs) is inevitable [1].

In weak power systems, it has been demonstrated that ESSs can drastically improve RES integration as well as network stability. On the other hand, it has been demonstrated that the stress applied on ESSs in such applications may significantly reduce their lifetime. Hybrid Energy Storage Systems (HESS) offer the possibility to increase the lifetime of each ESS as well as enhance the global specific power and specific energy of the whole system.

Unlike the 4W-3L-NPC topology, extensive studies have been carried out on HESS using parallel and floating power converter topologies. These topologies involve DC/DC converters that adapt ESSs voltages and control their power flow, leading to a lower global efficiency than the 3L-NPC topology [2]. The 3L-NPC topology also has less flexibility on the power flow control of each ESSs [3] and thus the power is limited and will depend on various factors including the DC voltage unbalances and the modulation index.

The 4th Leg of the inverter allows control of the neutral line to maintain a balanced voltage while in islanded mode and even in unbalanced load conditions. A literature review shows that the 4W-3L-NPC topology used as a unique power converter between a RES and a HESS to a microgrid has not been addressed.

This paper proposes an investigation of the limits of a 4W-3L-NPC when used as a HESS interface for RES integration to a microgrid. A second order sliding mode controller is then designed and tuned in order to control the power flow of the VRB and assess the limits of the topology in an operational scenario. The power division among each ESS is based on frequency decoupling, the fast load variations being supplied by the Li-Ion ESS and the trend by the VRB ESS. The 4th Leg of the converter makes it suitable to control the neutral line and therefore to maintain AC voltages balanced even with unbalanced load conditions.

2. MODELLING OF THE 4W-3L-NPC HESS INTERFACE

In this section, the ESSs models used in this work are described. Then the 4W-3L-NPC inverter model is developed and used to analyse the limits of the topology.

2.1. Modelling of the HESS

The HESS used in this work is composed of a Vanadium Redox Flow Battery (VRB) and a Lithium-Ion (Li-Ion) battery. These batteries have been selected for their high specific energy and specific power respectively, as well as for their very high round trip efficiencies of 65-88% for the VRB and 78-88% for the Li-Ion battery [4].

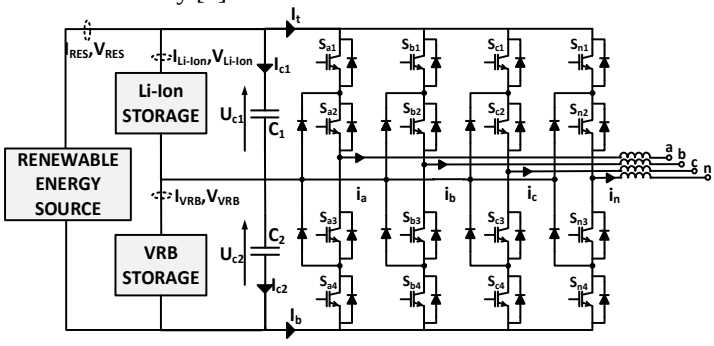

Fig. 1 4W-3L-NPC topology used as an HESS interface for RES integration

2.1.1. *Li-Ion ESS*

The Li-Ion model used in this work is based on the module presented in [5]. This model is already implemented in SimPowerSystems library of MATLAB/Simulink. The battery is realized with strings of series modules connected in parallel to build an ESS of 825 V/ 30Ah (at 80% of SOC and open circuit). The parameters of the Li-Ion battery are summed up in Table 1 and its equivalent circuit is presented in Fig. 2.

Table 1: Parameters of the Li-ion battery

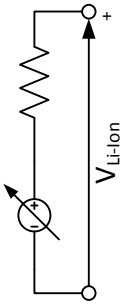

Parameter	Value
Cells in parallel	20
Cells in series	550
E_0 (V)	3.7348
K (V)	0.00876
A (V)	0.468
B $(Ah)^{-1}$	3.5294
R_s (Ω)	0.09

Fig. 2: Model of a Li-Ion cell

2.1.2. *Vanadium Redox Flow ESS*

The VRB used in this work has a rated voltage of 450V (at 50% of SOC and open circuit), a maximum charge/discharge current of 60A and a rated power of 25kW. The model of the VRB is based on the model introduced in [6], [7] and has been validated on a 1.25kW experimental device in [8]. Fig. 3 shows the equivalent circuit of the VRB whose parameters are summed up in Table 2.

Table 2: Parameters of the VRB unit

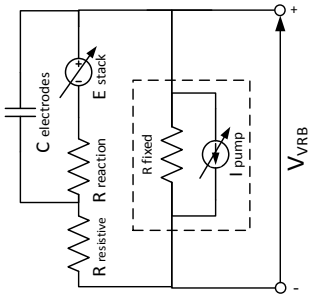

Parameter	Value
Cells in series	322
$V_{equilibrium}$ (V)	1.4
$R_{reaction}$ (Ω)	0.81
$R_{resistive}$ (Ω)	0.54
R_{fixed} (Ω)	295.
$C_{electrode}$ (F)	0.01

Fig. 3: Model of the VRB

2.2. *Modelling of the 4W-3L-NPC interface*

The 4W-3L-NPC topology used as a HESS interface is presented in Fig. 1. This topology has $4^3 = 64$ different switching states which produce different AC voltage vectors defined by (1). Vectors that can be generated by more than one switching state are called redundant vectors and allow power flow division control among the HESS [9] as they can be produce by one ESS or the other.

$$\overrightarrow{V_s} = \sqrt{\frac{2}{3}}\left[V_{an} + \vec{a}V_{bn} + \overrightarrow{a^2}V_{cn}\right] with\ \vec{a} = e^{\frac{j2\pi}{3}} \quad (1)$$

A zero sequence signal injected in the modulating signals allows the selection of the redundant vector and thus the control of the power division. This technique has been initially developed in order to balance the DC link capacitor voltages [10].

The 4th leg of the inverter allows control of the neutral line which makes the topology suitable for keeping a balanced voltage, even in unbalanced load conditions, while in isolated operation mode of a microgrid. The Three Dimensional Space Vector Modulation (3D-SVM) scheme is used to generate the 4th leg modulation signals [11].

Considering the average model of the 4W-3L-NPC converter, equation (2) represents the current as a function of the AC currents (where I_t is the current taken at the top level of the inverter and d_k^+ the modulating signals associated to this level).

$$I_t = i_a d_a^+ + i_b d_b^+ + i_c d_c^+ + i_n d_n^+ = i_{RES} + i_{Li\_Ion} + R_{Li\_Ion} C_2 \frac{di_{Li\_Ion}}{dt} - C_2 \underbrace{\frac{dE_{Li\_Ion}}{dt}}_{\approx 0} \quad (2)$$

The unbalanced AC voltages generated by unbalances in DC voltages are compensated using the factors in (3) to modify the modulating signals amplitude. The output AC waveforms are therefore not dependant on the ESSs voltages

$$A_1 = \frac{2V_{Li-Ion}}{V_{Li-Ion} + V_{vrb}}\ ;\ A_2 = \frac{2V_{vrb}}{V_{vrb} + V_{Li-Ion}} \quad (3)$$

Finally the modulating signals applied on the top half of the converter can be expressed as in (4) where Z_s is the zero sequence injection and d_k^{SVM} the modulating signals after the 3D SVM transform. The bottom side variables I_b and d_k^- can be obtained symmetrically.

$$d_k^- = \frac{A_1 - 1 + d_k^{SVM} + Z_s}{A_1}\ P_i \quad with\ P_i = \frac{1 + sign\left(\frac{A_1 - 1 + d_k^{SVM} + Z_s}{A_1}\right)}{2}\ and\ k = a, b, c, n \quad (4)$$

2.3. *Limits of the 4W-3L-NPC topology*

The limits of the topology will be investigated considering the DC link capacitor removed. The ratio of the mean power from one ESS on the RMS AC power is defined as the power division index and it can be expressed as in (3) for the Li-Ion battery. It can be symmetrically obtained for the VRB.

$$K_{Li\_Ion} = \frac{P_t}{P_{AC}} = \frac{I_t}{\frac{m}{2}\left(1 + \frac{V_{Li\_Ion}}{V_{vrb}}\right)\left(\frac{I_{a\,RMS} + I_{b\,RMS} + I_{c\,RMS}}{\sqrt{2}}\right)\cos(\varphi)} \quad (5)$$

It can be seen from (5) that the power division capabilities are clearly dependent on the DC voltage unbalances and the modulation index. Fig. 4 shows the evolution of the power division index depending on DC voltage unbalances and modulation index variations for maximum and minimum zero sequence injection (6). Power factor variations does not involve change in the limits on the contrary.

$$\begin{cases} Z_{s\,MAX} = 1 - |\max(d_k^{SVM})| \\ Z_{s\,MIN} = |\max(d_k^{SVM})| - 1 \end{cases} \quad (6)$$

Finally, if a RES injects a current on the DC bus, using (5) and Kirchhoff's laws, equation (7) that represents the lower and upper Li-Ion ESS power limit, with $K_{Li\_Ion}^{Z_s\,min/max}$ the power division index at minimum and maximum zero sequence injection.

$$P_{Li\_Ion}^{Z_s\,min/max} = -\frac{P_{res} A_1}{2} + K_{Li\_Ion}^{Z_s\,min/max}\ P_{AC} \quad (7)$$

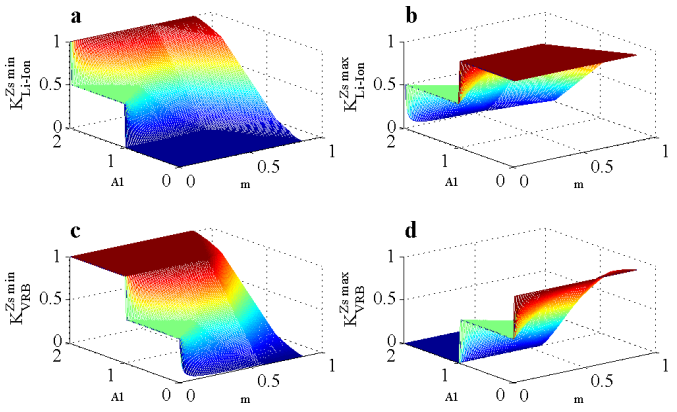

Fig. 4 Power division index for modulation index and DC voltage variations while: a) c) minimum b) d) maximum zero sequence injection.

Fig. 4Fig. presents the power division index for ESS voltage and modulation index variation. These surfaces represent the structural limits that each ESS can reach. Equation (7) can be then used to explore the limits that each ESS can reach while RES injection on the DC bus.

Using the power division behaviour defined in (7) , it can be seen that for a certain range of set points, it is possible to split the RES power between the AC load and the Li-Ion battery, while the rest of the AC power is provided by the other ESS. This phenomenon could be assimilated to an energy transfer from one ESS to another, and will be developed in Section 4 as a power exchange possibility between the ESSs is necessary for flexibility purpose in a HESS.

2.4. Limits and averaged model validation

The limits of the topology are assessed by simulation means using both averaged and detailed models of the converter. The ESSs are replaced by variable voltage sources and the RES by a current source injecting on the DC bus. To verify the effectiveness of the limits, the zero sequence signal injected is a sine varying from minimum to maximum according to (6) of 10Hz frequency. The RES power injected is a sine of 2kW amplitude and 1Hz frequency while the AC resistive load is increased at 2s to reach 2kW. The DC bus voltage is kept constant at 1kV but the ESSs voltages are varying with opposite sign.

Fig. 5 presents the result of this simulation. First it can be noted that there is an offset between the ESSs power detailed model compared to the averaged one. This is due to the losses that are not taken into account in the averaged model. It can also be seen that both ESSs power variations are within the limits calculated using (7) and displayed in green in c) and d). We can conclude from these results that the previous limits are valid for DC voltage, RES and AC load variations.

3. HESS CONTROL ARCHITECTURE AND DESIGN

3.1. DC side control

The DC side control aims to control the power flow of the VRB in order to smooth its power gradient. The control strategy is based on the Second Order Sliding Mode Control design principle using the Super Twisting Algorithm (STA) by Levant [12]. The design principle and tuning method is based on [13].

3.1.1. design of the controller

The chosen sliding function is the one shown in equation (8), where $e = \mathrm{i}_{\mathrm{vrb\ REF}} - \mathrm{i}_{vrb}$ and c is a positive constant.

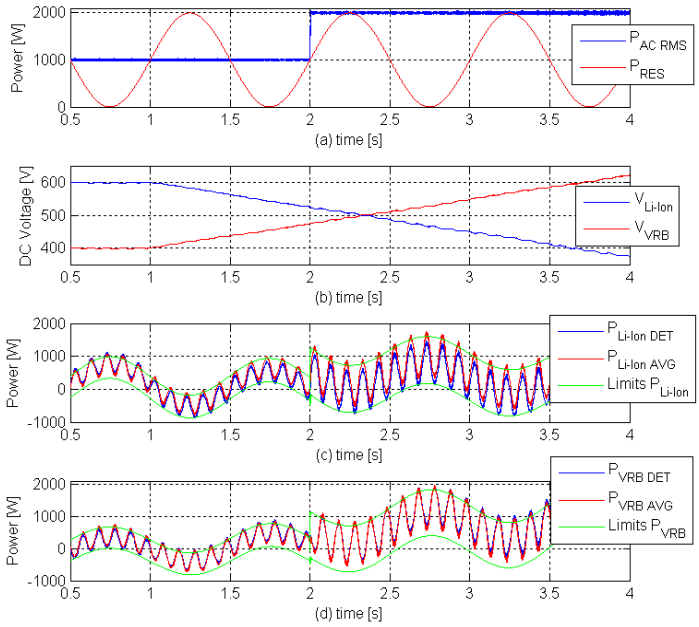

Fig. 5: ESSs Limits assessment while ESS voltage, RES power and load variation: a) AC and RES power b) ESSs voltages c) Li-Ion ESS power variation c) VRB ESS power variation.

$$s = e + c \int e\, dt \tag{8}$$

$$\frac{ds}{dt} = i_{vrb} + R_{vrb} C_2 \left(\frac{d\, i_{vrb\,REF}}{dt} + ce \right) - \sum_{k=a,b,c,n} \left[i_k \left(\frac{A_1 - 1 + d_k^* + Z_s}{A_2} \right) M_k + i_k \right] \tag{9}$$

Considering the structure of (9), the control law can be expressed as (10) where the term with the subscript 'ST' corresponds to the STA, and is given in (11) where λ and w are positive gains to be tuned. The first terms of (11) is used to guarantee s=0 is reached in finite time. The subscript 'EQ' corresponds to the equivalent control term obtained by letting $ds/dt = 0$ and is given in (12).

$$Z_s = Z_{s\,ST} + Z_{s\,EQ} \tag{10}$$

$$Z_{s\,ST} = \lambda \sqrt{|s|}\, sign(s) + w \int sign(s)\ dt \tag{11}$$

$$Z_{s\,EQ} = \frac{R_{vrb} C_2 \left(\frac{di_{vrb\,REF}}{dt} + c\, e \right) + i_{s2} - f_1}{f_2} \tag{12}$$

$$f_1 = \sum_{k=a,b,c,n} \frac{i_k M_k}{A_2} (A_1 - 1 + d_k^{SVM}) \tag{13}$$

$$f_2 = \sum_{k=a,b,c,n} \frac{i_k M_k}{A_2} \tag{14}$$

3.1.2. Tuning of the controller

Substituting the control law of (10), (11) and (12) into (9) results in equation (16).

$$\frac{ds}{dt} = -\frac{f_1}{R_{vrb}C_2}\left(\lambda\sqrt{|s|}\, sign(s) + w\int sign(s)\ dt\right) \qquad (15)$$

The f_1 function that appears in (15) and is given in (13) is hardly expressible as it uses variables from the AC side as well as the zero sequence injection. For the sake of simplicity, it is assumed that the f_1 function is constant and equal to its peak value on a given set point which is equal to the grid current peak value $\hat{f}_1$ divided by the DC voltage unbalance index A_2. Then, taking the time derivative of (15) and given that $sign(s) = s/|s|$ it comes (16).

$$\frac{d^2s}{dt^2} = -\frac{\hat{f}_1}{R_{VRB}C_2}\left(\frac{\lambda}{2\sqrt{|s|}}\frac{ds}{dt} + w\frac{s}{|s|}\right) \qquad (16)$$

Assuming the sliding mode is reached, we can consider $|s|<\Delta$, with Δ positive constant close to zero. Considering the worst case $|s|=\Delta$ and using the definition of s in (8), the following equation on the error comes to:

$$\frac{d^2e}{dt^2} + \underbrace{\left(\frac{\hat{f}_1\,\lambda}{2R_{VRB}C_2\sqrt{\Delta}} + c\right)}_{a_2}\frac{de}{dt} + \underbrace{\frac{\hat{f}_1}{R_{VRB}C_2\sqrt{\Delta}}\left(\frac{\lambda\, c}{2} + \frac{w}{\sqrt{\Delta}}\right)}_{a_1} e + \underbrace{\frac{\hat{f}_1\, w\, c}{R_{VRB}C_2\,\Delta}}_{a_0}\int e\ dt = 0 \qquad (17)$$

Taking the time derivative of (17), a third order equation (18) of the error dynamic while sliding mode is obtained.

$$\frac{d^3e}{dt^3} + a_2\frac{d^2e}{dt^2} + a_1\frac{de}{dt} + a_0\ e = 0 \qquad (18)$$

The error dynamic can then be identified with the third order transfer function defined in (19) in order to select appropriate c, λ and w gains. The identification leads to a set of parameters λ, w and several parameters c (20). The best parameter for c can be identified later by simulation means.

$$T_{fe} = (p^2 + 2\xi\omega_n\, p + \omega_n^2)(\mathrm{p} + \alpha\xi\,\omega_n) = p^3 + \underbrace{(2+\alpha)\,\xi\omega_n}_{a_2}p^2 + \underbrace{(1+2\alpha\xi^2)\omega_n^2}_{a_1}p + \underbrace{\alpha\xi\,\omega_n^2}_{a_0} \qquad (19)$$

$$\begin{cases} c = \omega_n \ or\ c = \alpha\omega_n \\ \lambda = \dfrac{2\,\pi\, R_{VRB}C_2\sqrt{\Delta}\left[(2+\alpha)\xi\,\omega_n - c\right]}{\hat{f}_1} \\ w = \dfrac{R_{VRB}C_2\,\Delta\,\alpha\,\xi\,\omega_n^3}{\hat{f}_1\, c} \end{cases} \qquad (20)$$

Given that $\alpha\omega_n \gg \omega_n$, the transfer function has a dominant pair of pole, typically $\alpha = 10$. For a damping ratio $\xi = 1$, the natural pulsation, and thus the whole error of the VRB current dynamic, can finally be defined only by the settling time t_s at 2%, as it is expressed by the approximation in (21).

$$\omega_n = -\frac{5.8}{t_s} \qquad (21)$$

3.2. AC side control

In a microgrid context, the global load is often unbalanced. As a consequence AC voltages could be significantly affected, especially in islanded mode. The investigated 4 Leg 3L-NPC inverter is able to take charge of such issues and keep AC voltages balanced, even in unbalanced load conditions, by using an adapted AC control. The control strategy used in this work is based on [14], which employs Fortescue's sequence decomposition in positive, negative and homopolar sequences, coupled with the 3D-SVM scheme to generate the 4th leg modulating signal. Each sequence is converted to the d-q rotating frame using the Park and Clark transforms and controlled independently using a classical double-loop PI scheme. The tuning of the used PI controller is based on pole placement with respect to an inner current loop settling time of 2ms and an outer voltage loop settling time of 4ms.

4. Simulation and Experimental Results

The simulations and experiment aims to verify the effectiveness of the proposed DC side power control as well as the limits of the topology. Simulations have been carried out for an inverter rated power of 100kW using Matlab/Simulink and the SimPowerSystems library. For laboratory purposes, the experiments have been carried out on a real scale prototype of 20kW but operating at few kW. Both simulation and experiment parameters are listed in Table 3.

Parameters	Simulation	Experiment
Switching frequency F_{sw}	10kHz	10kHz
AC RMS voltage L-N V_{ac}	230V	230V/2.2
AC filter L_f	6mH	3mH
DC filter C	6.6mF	3.3mF
VRB power settling time	0.25s	2.5s

Table 3: Parameters of the simulation and experimental test bench

4.1. VRB power reference definer

The VRB power reference definer implements the surface of Fig. 3 as well as equation (7) and gives the upper and lower bound that the VRB can reach. Fig. 6 shows a bloc representation of the VRB power definer where a reference selector allows selection of the maximum or minimum VRB power reference.

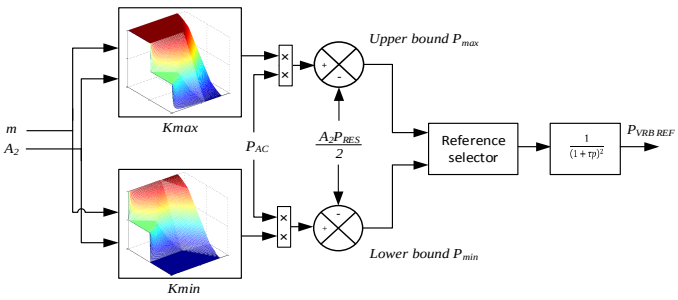

Fig. 6: VRB power reference definer

4.2. Case study simulation

To assess the ability of the converter to maintain a moderate power rate on the VRB as well as work at the limits offered by the topology, 5 cases studies have been combined in a unique scenario. The investigated scenario is composed of five sequences combining events on both AC and DC sides. The RES

injected into the DC bus is kept constant because RES variations can be considered as a perturbation equivalent to an AC load one, from a control point of view. The initial conditions and the events applied in the simulation are described in Table 4.

Case	Sequence/Event Desciption	Time
I	P_{ac}=40kW P_{res}=50kW P_{vrb_ref}= P_{vrb_max}	
Event 1	AC load step of 20kW	1s
II	P_{ac}=60kW P_{res}=50kW P_{vrb_ref}= P_{vrb_max}	
Event 2	VRB reference Max to Min	1.5s
III	P_{ac}=60kW P_{res}=50kW P_{vrb_ref}= P_{vrb_min}	
Event 3	AC load step of -20kW	2s
IV	P_{ac}=40kW P_{res}=50kW P_{vrb_ref}= P_{vrb_min}	
Event 4	10 kW monophasic load plugged	2.5s
V	P_{ac}=60kW P_{res}=50kW P_{vrb_ref}= P_{vrb_min}	

Table 4: Simulation scenarios and event description

Fig. 7 presents the result of a simulation with the ESSs models described in Section 2 on the detailed model of the inverter. It can be seen that the 2-SMC control scheme allows the VRB current to be maintained close to its reference, even if the AC load varies suddenly (Events 1 and 3) or is unbalanced (Case study V). The topology has a common mode voltage that involves a 150Hz current oscillations on the ESSs with a constant zero sequence injection. The amplitude of the oscillation strongly depends on the DC link filter parameters as well as the modulation type. However, thanks to the control of the VRB current, the oscillations of both ESS currents are compensated by the oscillation of the zero sequence injected.

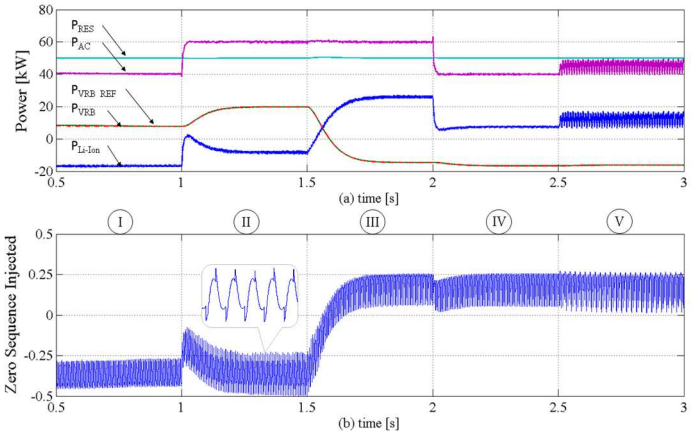

Fig. 7: Simulation results a) DC mean and AC RMS powers b) Zero sequence injected

4.3. Experimental Validation

The test bench employed for experimental validation shown in Fig. 8 is composed of the Opal-RT OP5600 real time simulator used to control the 4W-3L-NPC inverter, as well as two PAS1000 voltage amplifiers to emulate the ESSs and a third one as a current source injecting on the DC bus to emulate a RES. Due to laboratory limitation compared with the simulation tests, the voltages of the ESSs are divided by a factor of 2.2 and the peak voltage of the AC side is reduced by the same factor. The parameters of the experimental test bench are summed up in Table 3.

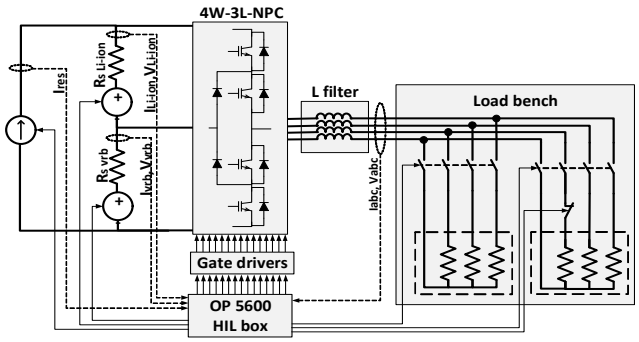

Fig. 8: Schematic of the experimental rig

The experimental results of the 2-SMC control strategy for the scenario and conditions summed up in Table 5 are shown in Fig. 9. As it can be seen there is a good agreement between simulation results shown in the previously and experimental results. The 2-SMC scheme allows the VRB current to be maintained close to its reference, even while the AC load varies or is unbalanced. The DC current oscillations are significantly reduced and the zero sequence injected has the expected profile too. It should also be noted that on both simulation and experiment and at specific set points, there is a phenomenon of power exchange between each HESS. At the end of the experiment's Case study III as an example, the power that has to be provided by the HESS (the difference between the AC power and the RES power) is 250W. However the Li-ion battery is injecting 750W and the VRB is charging at 500W approximately, which means that both HESS exchange in practice 500W. In reality the RES power is split between the AC load and the VRB, while the Li-Ion battery provide the rest of the power needed by the AC load. This ability to realise a kind of energy transfer from one ESS to another provide more flexibility to this topology used as an HESS interface in a microgrid context.

Cases	Sequence/Event Desciption	Time
I	P_{ac}=1kW P_{res}=1.5kW P_{vrb_ref}= P_{vrb_max}	
Event 1	AC load step of 750W	50s
II	P_{ac}=1.75kW P_{res}=1.5kW P_{vrb_ref}= P_{vrb_max}	
Event 2	VRB reference Max to Min	60s
III	P_{ac}=1.75kW P_{res}=1.5kW P_{vrb_ref}= P_{vrb_min}	
Event 3	AC load step of -750W	70s
IV	P_{ac}=1kW P_{res}=1.5kW P_{vrb_ref}= P_{vrb_min}	
Event 4	2 x 250W monophasic load plugged	80s
V	P_{ac}=1.5kW P_{res}=1.5kW P_{vrb_ref}= P_{vrb_min}	

Table 5: Experimental scenario and events description

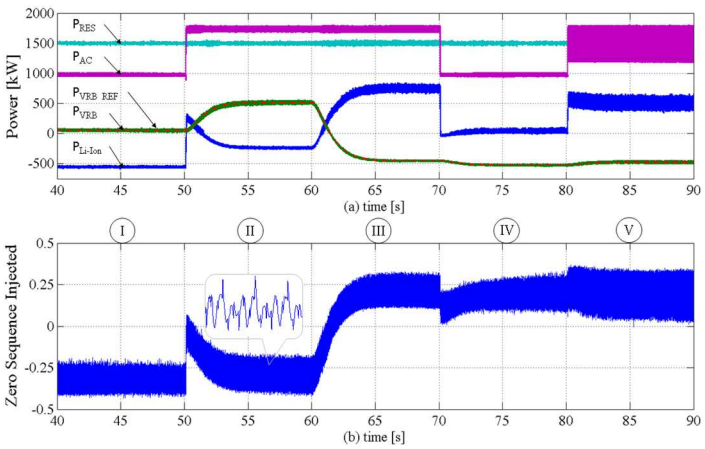

Fig. 9: Experimental results a) DC mean and AC RMS powers b) Zero sequence injected

5. CONCLUSIONS

In this paper the use of a 4W-3L-NPC power converter topology to manage a HESS (formed by a VRB and a Li-Ion battery) in a weak grid context has been presented. The fourth leg of this converter allows the unbalanced voltage problem to be addressed, keeping a balanced AC voltage even if the load is unbalanced. Furthermore, a 2-SMC scheme has been designed and tuned to control the zero sequence injection in the modulating signals in order to manage the power division among the ESSs. Simulation and experimental results proved the capacity of the proposed control strategy to significantly smooth the power taken from the VRB for longer lifetime expectancy, even in unbalanced load conditions. Despite the limited range of power division of the 4W-3L-NPC topology compared to other active topology, only one converter can be used to manage a HESS in order to improve the power quality and stability as well as the RES integration in a microgrid.

6. REFERENCES

[1] O. H. Anuta, P. Taylor, D. Jones, T. McEntee, and N. Wade, "An international review of the implications of regulatory and electricity market structures on the emergence of grid scale electricity storage," *Renew. Sustain. Energy Rev.*, vol. 38, pp. 489–508, Oct. 2014.

[2] A. Etxeberria, I. Vechiu, H. Camblong, and J.-M. Vinassa, "Comparison of three topologies and controls of a hybrid energy storage system for microgrids," *Energy Convers. Manag.*, vol. 54, no. 1, pp. 113–121, Feb. 2012.

[3] S. D. G. Jayasinghe, D. M. Vilathgamuwa, and U. K. Madawala, "A new method of interfacing battery/supercapacitor energy storage systems for distributed energy sources," in *IPEC, 2010 Conference Proceedings*, 2010, pp. 1211–1216.

[4] F. Díaz-González, A. Sumper, O. Gomis-Bellmunt, and R. Villafáfila-Robles, "A review of energy storage technologies for wind power applications," *Renew. Sustain. Energy Rev.*, vol. 16, no. 4, pp. 2154–2171, May 2012.

[5] O. Tremblay, L.-A. Dessaint, and A.-I. Dekkiche, "A Generic Battery Model for the Dynamic Simulation of Hybrid Electric Vehicles," in *2007 IEEE Vehicle Power and Propulsion Conference*, 2007, no. V, pp. 284–289.

[6] L. Barote, C. Marinescu, and M. Georgescu, "VRB modeling for storage in stand-alone wind energy systems," in *PowerTech, 2009 IEEE Bucharest*, 2009, pp. 1–6.

[7] J. Chahwan, C. Abbey, and G. Joos, "VRB modelling for the study of output terminal voltages, internal losses and performance," *2007 IEEE Canada Electr. Power Conf. EPC 2007*, pp. 387–392, Oct. 2007.

[8] I. Vechiu, A. Etxeberria, H. Camblong, and Q. Tabart, "Control of a microgrid-connected hybrid energy storage system," in *Renewable Energy Research and Application (ICRERA), 2014 International Conference on*, 2014, pp. 412–417.

[9] S. S. G. Jayasinghe, D. M. Vilathgamuwa, and U. K. Madawala, "Diode-Clamped Three-Level Inverter-Based Battery/Supercapacitor Direct Integration Scheme for Renewable Energy Systems," *IEEE Trans. Power Electron.*, vol. 26, no. 12, pp. 3720–3729, Dec. 2011.

[10] N. Celanovic and D. Boroyevich, "A comprehensive study of neutral-point voltage balancing problem in three-level neutral-point-clamped voltage source PWM inverters," *IEEE Trans. Power Electron.*, vol. 15, no. 2, pp. 242–249, Mar. 2000.

[11] M. A. Perales, M. M. Prats, R. Portillo, J. L. Mora, J. I. Leon, and L. G. Franquelo, "Three-dimensional space vector modulation in abc coordinates for four-leg voltage source converters," *IEEE Power Electron. Lett.*, vol. 1, no. 4, pp. 104–109, Dec. 2003.

[12] A. Levant, "Sliding order and sliding accuracy in sliding mode control," *Int. J. Control*, vol. 58, no. 6, pp. 1247–1263, 1993.

[13] a. Susperregui, M. I. Martinez, I. Zubia, and G. Tapia, "Design and tuning of fixed-switching-frequency second-order sliding-mode controller for doubly fed induction generator power control," *IET Electr. Power Appl.*, vol. 6, no. 9, p. 696, 2012.

[14] I. Vechiu, O. Curea, and H. Camblong, "Transient Operation of a Four-Leg Inverter for Autonomous Applications With Unbalanced Load," *IEEE Trans. Power Electron.*, vol. 25, no. 2, pp. 399–407, Feb. 2010.